

# Gravitational microlensing of quasar Broad Line Regions: the influence of fractal structures

Geraint F. Lewis<sup>1</sup> & Rodrigo A. Ibata<sup>2</sup>

<sup>1</sup>*Institute of Astronomy, School of Physics, University of Sydney, NSW 2006, Australia: gfl@physics.usyd.edu.au*

<sup>2</sup>*Observatoire de Strasbourg, 11 Rue de l'Université, F-6700 Strasbourg, France: ibata@astro.u-strasbg.fr*

27 September 2018

## ABSTRACT

Recent models for the emission clouds within the Broad Line Region of quasars suggest that they are due to transient overdensities within an overall turbulent medium. If this were the case, the broad line emission would spatially appear fractal, possessing structure on a range of scales. This paper examines the influence of such fractal structure when a quasar is microlensed by a population of intervening masses. It is found that while the highest fractal levels can undergo significant microlensing magnification, when these light curves are superimposed to create an emission line profile, the resultant emission line profile remains relatively constant for physical models of the Broad Line Region. It is concluded that the detection of the possible fractal structure of Broad Line Regions via gravitational microlensing is not practical.

**Key words:** gravitational lensing – quasars: emission lines – quasars: absorption lines

## 1 INTRODUCTION

While quasars are amongst the most luminous objects in the Universe, the majority of their emission is generated within a region only parsecs in extent. At cosmological scales, such regions are well below the resolving power of even the most powerful telescopes, and so the spatial structure within these inner regions cannot be directly observed and must be inferred by other, more indirect means.

In recent years, a general picture for quasar central regions has emerged, with a hot accretion disk surrounding a supermassive black hole being responsible for the extensive continuum emission characteristic of quasars. Beyond this, on the scale of  $\sim 1pc$ , this accretion disk is surrounded by a large population of clouds which are illuminated by the central engine and produce the broad emission lines, with widths of thousands of  $\text{km s}^{-1}$ , also characteristic of quasar spectra<sup>1</sup>.

Initial studies of the Broad Line Region (BLR) were based on simple ionisation models, with predicted BLR sizes of 0.1 to a few parsecs in extent (e.g. Davidson & Netzer 1979). Recent studies, utilising reverberation mapping to measure the scale of the BLR, how-

ever, have found evidence for a smaller BLR, more than an order of magnitude smaller than suggested by ionisation models (Peterson, Crenshaw, & Meyers 1985). Furthermore, Wandel, Peterson, & Malkan (1999) and Kaspi et al. (2000) have demonstrated that the size of the BLR scales with quasar luminosity, with  $R_{BLR} \propto L^{0.7}$ , and BLRs were also found to possess significant ionisation stratification, with high-ionisation lines arising in a region an order of magnitude smaller than low-ionisation lines.

The origin of the BLR has proved problematic to understand, with suggestions that the emitting material could be the debris from star-disk collisions at the heart of the quasar (Zurek, Siemiginowska, & Colgate 1994; Armitage, Zurek, & Davies 1996), supernova explosions within quasar outflows (Pittard et al. 2001, 2003), or even the bloated atmospheres of irradiated stars (Alexander & Netzer 1997). However, the BLR must possess significant substructure, with line emission arising from dense clouds embedded in a lower density medium (Capriotti, Foltz, & Byard 1981), with the smoothness of emission lines suggesting that there must be of order  $10^8$  emitting clouds (Arav et al. 1998), effectively ruling out the picture of the BLR being composed of a relatively small number of large clouds or bloated stars. Nevertheless, such a situation is physically problematic, as these clouds should rapidly dissipate, with various mechanisms suggested for their confinement [e.g. magnetic fields Rees (1987)].

Recently, Bottorff & Ferland (2001) suggested that the

<sup>1</sup> It should be noted that alternative models for the source of the broad line emission exist, including the accretion disk wind model of Murray et al. (1995) which occurs on a considerably smaller scale.

‘clouds’ within the BLR are not isolated, individual entities embedded within a confining medium, but rather represented transient knots of higher density within an overall turbulent BLR. One conclusion of this study was that the BLR would not appear as a smoothly-varying emitting region. Instead, the turbulent nature of the BLR would result in the spatial emission from the region possessing an overall fractal structure.

Gravitational microlensing provides an opportunity to ‘see’ the structure in the central regions of quasars, utilising differential magnification effects (Wambsganss & Paczynski 1991). Recently, Lewis (2004) demonstrated that small-scale fractal structures within quasars, arising in an x-ray emitting hot corona above the accretion disk, imprint themselves on the light curve of a microlensed quasar. Hence, this paper considers the influence of microlensing on an extended, fractal BLR. However, as this is more extensive than the X-ray emitting region, it is important to compare it to the natural scale length for gravitational microlensing; the Einstein radius. In the source plane, this is given by

$$\eta = \sqrt{4 \frac{GM}{c^2} \frac{D_{ls} D_{os}}{D_{ol}}} \quad (1)$$

where  $M$  is the mass of the microlensing body, and  $D_{ij}$  are angular diameter distances between the observer ( $o$ ), lens ( $l$ ) and source ( $s$ ). For typical cosmological lensing configurations, with microlensing stars with mass  $M \lesssim 1 M_{\odot}$ , this scale length is  $\eta \lesssim 0.1 \text{pc}$ , and is often substantially smaller. The X-ray emitting region considered in Lewis (2004) is small compared to this scale and hence significant microlensing magnification is expected. As discussed in Lewis & Ibata (2004), however, the extensive nature of the BLR ensures it must lie across a substantial portion of the complex caustic network that is seen at high optical depths, and the effects of microlensing cannot be approximated by the influence of individual caustic structures. The structure of this paper is as follows; Section 2 describes the numerical approach adopted in this study, while Section 3 discusses the resultant microlensing light curves and their statistical properties. The conclusions to this study are presented in Section 4.

## 2 METHOD

### 2.1 Cloud Distributions

The argument that BLRs possess fractal structure was expounded by the turbulence model of Bottorff & Ferland (2001), and it is this procedure for defining a fractal cloud distribution that is utilised in this paper. The fractal structure occupies a region with an overall scale size of  $R_{max}$ . Within this radius there are a series of hierarchies whose radius is given by

$$R(h) = R_{max} L^{-h} \quad (2)$$

where  $h = 0, 1 \dots H$  is the level of the hierarchy,  $H$  denotes the maximum fractal hierarchy in the structure and  $L$  is a geometric factor. Each hierarchy possesses  $N$  substructures (the multiplicity) and the overall fractal dimension is defined to be

$$D = \frac{\log N}{\log L} \quad (3)$$

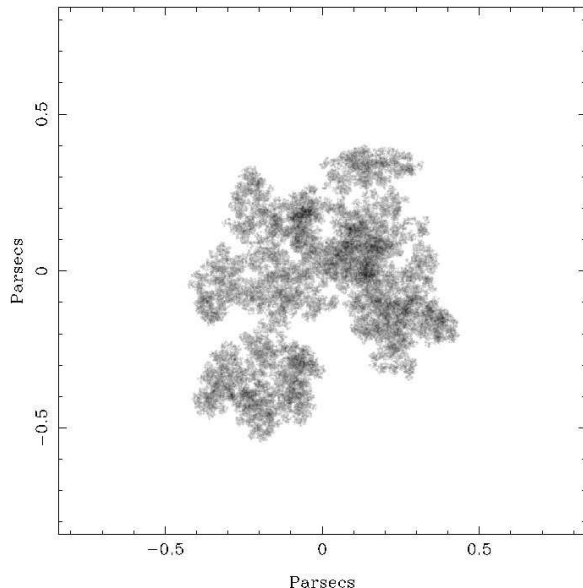


**Figure 1.** A realisation of a fractal BLR as described in Bottorff & Ferland (2001). Clearly clumps and subclumps can be seen, but the smallest structures in this picture ( $\sim 10^{-6} \text{pc}$ ) are too small to be seen by eye.

To generate a fractal distribution, a region  $R_{max}$  is defined; this is the zeroth level of the hierarchy with  $h = 0$ . Within this region,  $N$  locations are chosen at random and represent the centres of the first level of the hierarchy (with  $h = 1$ ) and assigned a radius given by Equation 2. Within each individual subregion, a further  $N$  centres are scattered at random and are assigned a radius corresponding to the second level of the hierarchy, with  $h = 2$ . The process is continued until the highest level of the hierarchy,  $h = H$  is reached; each point in this upper-most hierarchy corresponds to the location of a cloud with a radius given by Equation 2. This procedure results in a total of  $n_{tot} = N^H$  clouds being distributed over a region. For the purposes of this study, each of these final clouds was assumed to have the same luminosity, although a more realistic model would probably require a distribution of luminosities throughout the region.

In considering a realistic model for the BLR Bottorff & Ferland (2001) determined the fractal parameters required to reproduce known physical properties of the region, such as its column density and covering factor. These values are employed in this current study, with  $R_{max} = 5.12 R_{BLR}$ , where  $R_{BLR}$  is the nominal radius to the BLR,  $L = 3.2$  and  $N = 14$  (see footnote 2). The maximum hierarchy which will be employed is related to the resolution of the microlensing magnification map, which is discussed in Section 2.2.

In choosing  $R_{BLR}$ , the scale relation between the BLR radius and the luminosity of the quasar, as derived from reverberation mapping is employed (Wandel, Peterson, & Malkan 1999; Kaspi et al. 2000). As discussed in the next section, this study will focus on the

<sup>1</sup> In the study of Bottorff & Ferland (2001),  $N = 14.62$ , and fractal structures could be generated by drawing the number in a particular hierarchy with this being the mean value. Fixing  $N = 14$  does not significantly influence the resulting fractal structure.

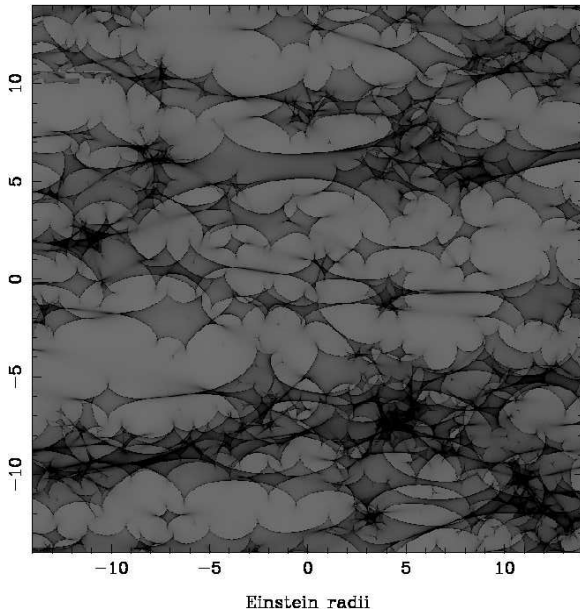


**Figure 2.** The magnification map employed in this study. Representing image A of the microlensed quasar, Q2237+0305, a dimensionless surface density of  $\kappa = 0.36$  and external shear of  $\gamma = 0.41$  were employed. The units are in Einstein radii for a solar mass star and the scale of the image matches that presented in Figure 1.

microlensed images of the quasar Q2237+0305, which possess an absolute magnitude of  $M \sim -26$  [accounting for a magnification of  $\sim 16$  (Schmidt, Webster, & Lewis 1998)]; as shown in (Lewis & Iбата 2004) this corresponds to a  $R_{BLR} \sim 0.05\text{pc}$  for high-ionization emission (e.g. C IV) and  $R_{BLR} \sim 0.4\text{pc}$  for low-ionisation emission (e.g. Mg II). For the purposes of this study,  $R_{BLR} = 0.1\text{pc}$ , a value between the high and low emission scale sizes. Using these parameters, a typical fractal BLR can be generated, with an example presented in Figure 1.

## 2.2 Gravitational Microlensing

As noted in Section 1, the substantial size of the BLR implies that the influence of gravitational microlensing cannot be approximated as a simple point-mass lens or isolated caustic structure. To this end, the backward ray-tracing approach of Kayser et al. (1986) and Wambsganss et al. (1990) was used to generate the magnification map employed in this study.

The macrolensing parameters were chosen to represent Image A of Q2237+0305, the most intensively-studied microlensed quasar, with a dimensionless surface mass density of  $\kappa = 0.36$  and an external shear of  $\gamma = 0.41$ ; this surface mass density describes the focusing due to matter within the beam of light traversing the galaxy, whereas the shear is the distortion of the beam due to the larger scale distribution of matter (Kayser et al. 1986). All of the mass is distributed in microlenses with masses of  $1M_{\odot}$ . Given that the lensing galaxy in this system possesses a redshift of  $z_l = 0.0395$ , while the source quasar is at  $z_s = 1.695$ , the Einstein Radius (Equation 1) for a solar mass star is  $\eta_o \sim 0.06\text{pc}$ , adopting the current concordance cosmology. To accommodate the model BLR described in Section 2.1, the entire ray trac-

ing region is taken to be 28 Einstein radii ( $\sim 1.68\text{pc}$ ) on a side. The resulting magnification map used in this study is presented in Figure 2.

## 2.3 Image pixelation

Clearly, the fractal clouds outlined in Section 2.1 possess structure on a range of scales and this must be reflected in the magnification map. Hence the magnification map utilised in this study possesses a pixel scale of 1000 pixels per Einstein Radius, with one pixel physically corresponding to  $6 \times 10^{-5}\text{pc}$ , and the total map presented in Figure 2 is 28000 pixels on a side. If a pixel in this map represents a single cloud in the fractal BLR, then the maximum hierarchy in the fractal distribution corresponds to  $H \sim 7$  and the total number of clouds in the BLR is  $N_{tot} \sim 1.5 \times 10^9$ . Note that the model of Bottorff & Ferland (2001) considered a maximum fractal hierarchy of  $H = 11$ , with a total of  $N_{Tot} \sim 4 \times 10^{14}$  individual clouds; with this, the scale of each cloud would be  $\sim 1.4 \times 10^{-6}\text{pc}$  and the magnification map presented in Figure 2 would have to be  $1.2 \times 10^6$  pixels along each side, a very challenging prospect. As discussed later, the lower resolution map adopted here does not significantly influence the conclusions of this paper.

## 2.4 Generating light curves

In typical gravitational microlensing problems, magnification maps are convolved with the surface brightness profile of a preferred source, providing a map from which the microlensing light curve from that source can be drawn. Such a convolution, utilising Fourier transform techniques, was found to be computationally too expensive, given the number of pixels used in the magnification map. Hence, in this present study, light curves were simply generated by extracting a single column of pixels along a magnification map at the location of a BLR cloud. Summing each of these columns for a collection of clouds together then gives the overall light curve of the BLR region of interest. With this approach, each individual BLR cloud (the smallest structure within the entire BLR) has a size of a single pixel in the map, corresponding to  $6 \times 10^{-5}\text{pc}$ .

## 3 RESULTS

Figure 3 presents a series of light curves derived from this analysis. Each panel presents subsections of the fractal hierarchy, from  $h = 7$  in the top-left, consisting of a total of 14 sources), to  $h = 0$  in the bottom-right, with a total of  $1.5 \times 10^9$  clouds. The background of each panel presents a greyscale map of the fractal structure (note in  $h = 7$  and  $h = 6$  the structure is too small to see). Each subpanel presents the microlensing light curve for the fractal hierarchy; the x-axis is in units of Einstein radii, whereas the y-axis corresponds to the magnification of the region. The expected crossing time of an Einstein radius in this system (assuming a transverse velocity of the lens of  $\sim 600\text{km/s}$ ) is  $\sim 8$  yrs (e.g. Lewis & Irwin 1996). The degree of variability changes quite strongly with fractal hierarchy  $h = 7$  displaying the strong variability, with caustic crossings quite

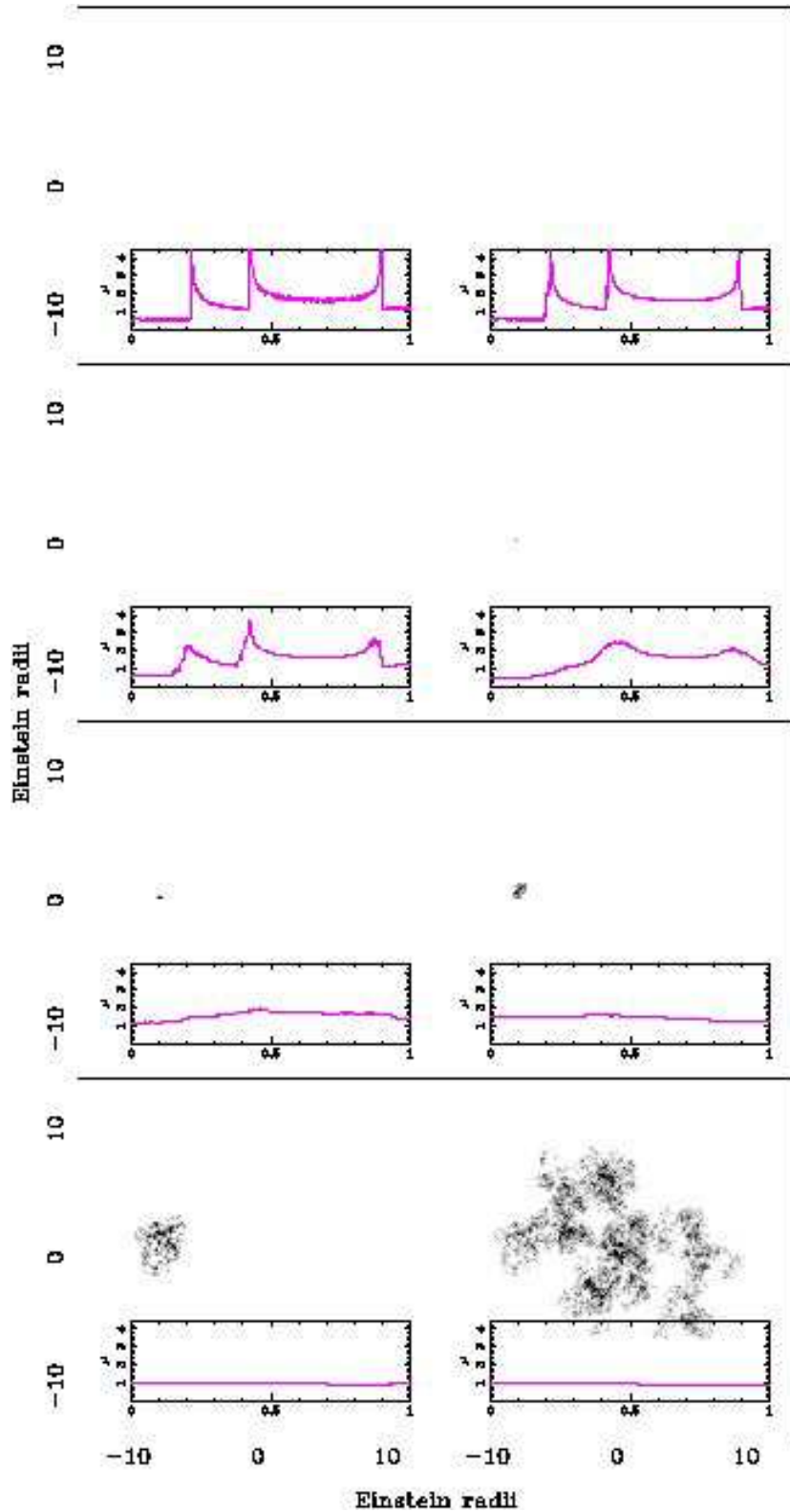


**Figure 3.** Example light curves for the fractal hierarchies presented in this paper, from the smallest ( $h = 7$  top-left) to the largest ( $h = 0$  bottom-right). Each panel presents the cloud distribution (note that the smallest structures are not visible on the scale of these figures), with the resulting light curve arising from the magnification map presented in Figure 2. Each light curve is 1 Einstein radii in extent, with the location of the clouds in the figure representing the centre of the position at the centre of the light curve.

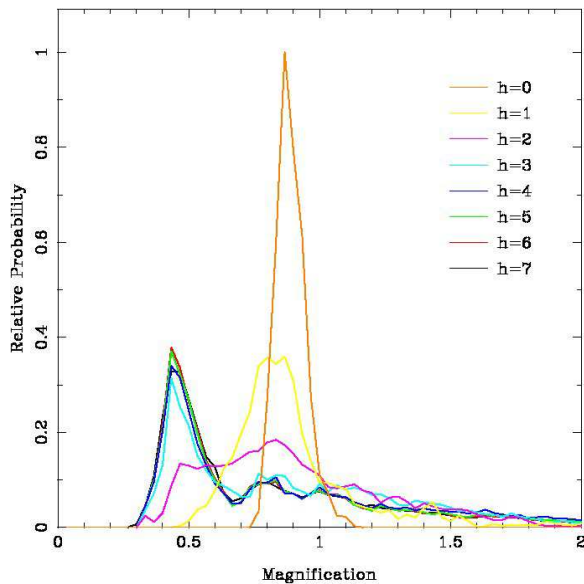


**Figure 4.** The magnification distributions for 250 realisations of fractal BLRs combined with the magnification map displayed in Figure 2.

similar to point-like sources<sup>2</sup>. Clearly these source sizes at fractal hierarchies of  $h > 7$  are substantially smaller than the fractal structure seen in Figure 2 and hence the resulting light curves for individual sources at this level would appear qualitatively the same as the  $h = 7$  case, although the peak magnifications would be larger. Considering lower values of  $h$ , it can be seen that the light curve fluctuations are smoothed out, as expected as the source size increases (Wambsganss & Paczynski 1991), while at the base fractal level ( $h = 0$ ), which considers the entire cloud population, the light curve is quite flat.

To examine this further, 250 light curve samples were generated with differing realisations of the fractal hierarchy. Figure 4 presents the magnification probability distributions for each of the fractal hierarchies in the entire sample. These confirm the properties of the light curve seen in Figure 3, with the highest fractal hierarchy displaying magnifications of 10 – 20%. This distribution is quite different to the lower fractal hierarchies which display typical light curves for small sources. Here the magnification probability distribution is dominated by a peak at a magnification of 0.5, corresponding to extensive periods of demagnification in the light curve, with a high magnification tail representing the periods of caustic crossing (Wambsganss 1992; Lewis & Irwin 1995).

A simple interpretation of this result, therefore, is that if BLRs do indeed possess the fractal structure outlined, then, on the whole, they should not be significantly magnified by gravitational microlensing. While this is true, what it actually implies is that the total flux in the emission line will not vary as the quasar is microlensed, but it must be remembered that as well as spatial structure, BLRs also possess kinematic structure which is responsible for the width

of the emission line [see earlier studies by Nemiroff (1988) and Schneider & Wambsganss (1990)].

As noted in Bottorff & Ferland (2001), however, the fractal BLR model they present is purely geometrical and does not consider the kinematic aspects of the BLR. For the purposes of this paper, a toy model for the kinematic properties is considered, with clouds of a particular fractal hierarchy assigned a velocity drawn from a Keplerian distribution with random projections (i.e. all clouds at a particular fractal hierarchy and above are assigned the same projected velocity). This velocity structured BLR was then microlensed and the light curves summed into kinematic bins. The results of this exercise are presented in Figure 5; the left-hand panels present the emission line profile, comprised of 1000 velocity elements, whereas the right-hand panel presents the light curves for sampled values of the velocity elements over one Einstein radius. The spread in the emission line profile represents the superposition of all emission lines along the one Einstein radius. The pairs of panels arranged vertically represent the various velocity models; i.e. in the  $h = 7$  model, each of the 14 clouds within the highest fractal hierarchy are assigned the same Keplerian velocity, for  $h = 6$ ,  $14^2$  within the second highest are assigned the same Keplerian velocity, etc. Clearly, the  $h = 7$  emission line profile displays very little variability. Even at this high resolution, each velocity element must be the sum of of the light curves of many small sources, averaging out to give an overall flat light curve. In moving to lower fractal hierarchies, the emission line profiles display more and more variability. However, it is clear that bulk motions of the lowest fractal hierarchies result in very “choppy” structure, with the  $h = 2$  emission line breaking down into a series of spikes. The smoothness of observed emission lines suggest that such a situation is unphysical (e.g. Arav et al. 1998) and hence the kinematic properties must be defined by the higher fractal hierarchies. It can be concluded, therefore, that the fractal structure will be virtually impossible to detect by studying the emission line profiles of microlensed quasars.

## 4 CONCLUSIONS

The nature of the broad line emission regions of quasars has remained a subject of discussion for a number of years, with recent models suggesting that the emitting clouds are temporary density enhancements in an overall turbulent medium. Such a scenario predicts that these density enhancements should have a fractal distribution of structures. This paper has investigated the influence of gravitational microlensing on this extensive fractal structure, finding that different levels of the fractal structure undergo differing magnifications, with the smaller sections of the substructure suffering stronger magnification. It was found, however, that while individual clouds in the fractal hierarchy displayed quite dramatic variability due to microlensing, the combination of light curves from the entire population of clouds within the BLR resulted in an overall constant light curve.

While the overall magnification of the BLR appears to be constant, more significant magnification of substructures could be apparent when examining the form of the emission line profile, i.e. substructures within the BLR could possess coherent velocities and hence may contribute to a

<sup>2</sup> The slight fuzz visible in the light curve is due to low-level numerical noise in the magnification maps. Its presence does not influence the results of this study.

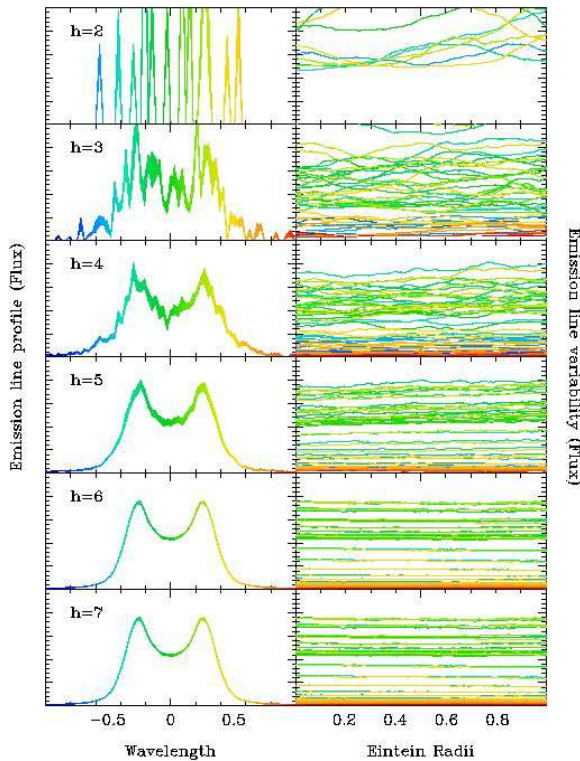


**Figure 5.** The emission line profile for the toy kinematic models presented in this paper. The left-hand panel presents the emission line profile for the appropriate bulk motion of the fractal structure. The right-hand panel presents the light curve for various portions of the lines, colour-coded to match the wavelengths presented in the left-hand panels. In this figure, the total fractal hierarchy is the same for all frames and the  $h$  values denote the hierarchy at which the bulk velocity has been assigned; i.e. in the top panel with  $h = 2$ , each  $h = 2$  has been assigned a velocity drawn from the model and this value has been assigned to each higher fractal level within that  $h = 2$  structure. Hence the  $h = 7$  possesses more kinematic diversity than  $h = 2$ , resulting in the overall smoothness of the resulting emission line.

particular velocity within the emission line. This paper considered a simple Keplerian velocity structure for the emission line clouds, assigning a particular velocity to all fractal hierarchies below a particular level. The result of this procedure, however, revealed that coherent velocity structure cannot apply to the lowest levels of the fractal hierarchy as the resultant emission line profile is clearly too structured, although dramatic variability is seen throughout the line. Assigning coherent velocity structure to the higher fractal hierarchy does smooth out the form of the emission line, but it also smooths out the light curves for each velocity bin. From this it is possible to conclude that while individual structures within a BLR are being microlensed and are undergoing significant magnifications, the extensive nature of the BLR and the requirement that the resulting emission line appears relatively smooth means that microlensing is unlikely to reveal the putative fractal structure of quasar BLRs.

## REFERENCES

- Abajas C., Mediavilla E., Muñoz J. A., Popović L. Č., Oscoz A., 2002, *ApJ*, 576, 640
- Alexander T., Netzer H., 1997, *MNRAS*, 284, 967
- Arav N., Barlow T. A., Laor A., Sargent W. L. W., Blandford R. D., 1998, *MNRAS*, 297, 990
- Armitage P. J., Zurek W. H., Davies M. B., 1996, *ApJ*, 470, 237
- Bottorff M., Ferland G., 2001, *ApJ*, 549, 118
- Capriotti E., Foltz C., Byard P., 1981, *ApJ*, 245, 396
- Davidson K., Netzer H., 1979, *RvMP*, 51, 715
- Kaspi S., Smith P. S., Netzer H., Maoz D., Jannuzi B. T., Giveon U., 2000, *ApJ*, 533, 631
- Kayser R., Refsdal S., Stabell R., 1986, *A&A*, 166, 36
- Lewis G. F., 2004, *MNRAS*, 355, 106
- Lewis G. F., Ibata R. A., 2004, *MNRAS*, 348, 24
- Lewis G. F., Irwin M. J., 1995, *MNRAS*, 276, 103
- Lewis G. F., Irwin M. J., 1996, *MNRAS*, 283, 225
- Mediavilla E., et al., 1998, *ApJ*, 503, L27
- Murray N., Chiang J., Grossman S. A., Voit G. M., 1995, *ApJ*, 451, 498
- Nemiroff R. J., 1988, *ApJ*, 335, 593
- Peitgen, H.-O., Saupe, D., 1988, *The Science of Fractal Images*, Springer-Verlag (Berlin)
- Peitgen, H.-O., Richter, P. H., 1986, *The Beauty of Fractals*, Springer-Verlag (Berlin)
- Peterson B. M., Crenshaw D. M., Meyers K. A., 1985, *ApJ*, 298, 283
- Pittard J. M., Dyson J. E., Falle S. A. E. G., Hartquist T. W., 2003, *A&A*, 408, 79
- Pittard J. M., Dyson J. E., Falle S. A. E. G., Hartquist T. W., 2001, *A&A*, 375, 827
- Rees M. J., 1987, *MNRAS*, 228, 47P
- Schmidt R., Webster R. L., Lewis G. F., 1998, *MNRAS*, 295, 488
- Schneider P., Wambsganss J., 1990, *A&A*, 237, 42
- Wambsganss J., 1992, *ApJ*, 386, 19
- Wambsganss J., Paczynski B., 1991, *AJ*, 102, 864
- Wambsganss J., Paczynski B., Katz N., 1990, *ApJ*, 352, 407
- Wandel A., Peterson B. M., Malkan M. A., 1999, *ApJ*, 526, 579
- Wayth, R. B., O'Dowd, M., Webster, R. L., 2005, *MNRAS*, *Accepted*, *astro-ph/0502396*
- Zurek W. H., Siemiginowska A., Colgate S. A., 1994, *ApJ*, 434, 46